Modelling the Venusian airglow

Guillaume Gronoff, Jean Lilensten, Cyril Simon, Mathieu Barthélemy, François Leblanc, Odile Dutuit

▶ **To cite this version:**

Guillaume Gronoff, Jean Lilensten, Cyril Simon, Mathieu Barthélemy, François Leblanc, et al.. Modelling the Venusian airglow. Astronomy and Astrophysics - A&A, 2008, 482 (3), pp.1015-1029. 10.1051/0004-6361:20077503 . hal-00275449

HAL Id: hal-00275449
https://hal.science/hal-00275449

Submitted on 16 May 2019

HAL is a multi-disciplinary open access archive for the deposit and dissemination of scientific research documents, whether they are published or not. The documents may come from teaching and research institutions in France or abroad, or from public or private research centers.

L'archive ouverte pluridisciplinaire **HAL**, est destinée au dépôt et à la diffusion de documents scientifiques de niveau recherche, publiés ou non, émanant des établissements d'enseignement et de recherche français ou étrangers, des laboratoires publics ou privés.

A&A 482, 1015–1029 (2008)
DOI: 10.1051/0004-6361:20077503
© ESO 2008

Astronomy & Astrophysics

Modelling the Venusian airglow

G. Gronoff[1], J. Lilensten[1], C. Simon[1,2], M. Barthélemy[1], F. Leblanc[3], and O. Dutuit[1]

[1] Laboratoire de Planétologie de Grenoble, Université Joseph Fourier - CNRS, France
e-mail: guillaume.gronoff@obs.ujf-grenoble.fr
[2] Research and Scientific Support Department of ESA, ESTEC, Noordwijk, The Netherlands
[3] Service d'aéronomie du CNRS/IPSL, Verrières-le-Buisson, France

Received 19 March 2007 / Accepted 5 February 2008

ABSTRACT

Context. Modelling of the Venusian ionosphere fluorescence is required, to analyse data being collected by the SPICAV instrument onboard Venus Express.
Aims. We present the modelling of the production of excited states of O, CO and N_2, which enables the computation of nightglow emissions. In the dayside, we compute several emissions, taking advantage of the small influence of resonant scattering for forbidden transitions.
Methods. We compute photoionisation and photodissociation mechanisms, and the photoelectron production. We compute electron impact excitation and ionisation, through a multi-stream stationary kinetic transport code. Finally, we compute the ion recombination using a stationary chemical model.
Results. We predict altitude density profiles for $O(^1S)$ and $O(^1D)$ states, and emissions corresponding to their different transitions. They are found to agree with observations. In the nightside, we discuss the different $O(^1S)$ excitation mechanisms as a source of green line emission. We calculate production intensities of the $O(^3S)$ and $O(^5S)$ states. For CO, we compute the Cameron bands and the Fourth Positive bands emissions. For N_2, we compute the LBH, first and Second Positive bands. All values are compared successfully to experiments when data are available.
Conclusions. For the first time, a comprehensive model is proposed to compute dayglow and nightglow emissions of the Venusian upper atmosphere. It relies on previous works with noticeable improvements, both on the transport side and on the chemical side. In the near future, a radiative-transfer model will be used to compute optically-thick lines in the dayglow, and a fluid model will be added to compute ion densities.

Key words. planets and satellites: individual: Venus – atmospheric effects – Sun: UV radiation – space vehicles: instruments

1. Introduction

Venus ultraviolet emissions have been studied for decades, by spacecrafts such as Pioneer Venus Orbiter (PVO), or space observatories such as Astro-2 (Feldman et al. 2000; Fox & Dalgarno 1981). A review of the modelling and observations of these emissions, can be found in Fox & Bougher (1991). The oxygen green line was discovered in the nightside of Venus (Slanger et al. 2001), opening a controversy about its origin. A mesospheric origin was suggested by an unobserved high vibrational O_2^* state, or an unobserved quenching reaction. In the present paper, we present a new code called TRANS-VENUS, which is one of the first multi-stream codes on Venus providing a new insight on these phenomena.

2. The production model TRANS-VENUS

The production of ions and excited states is based on the telluric kinetic part of TRANSCAR (Lilensten & Blelly 2002), called TRANSSOLO. The Venusian version was described in Gronoff et al. (2007). This code was adapted for Mars (Witasse 2000; Witasse et al. 2002, 2003), and Titan (Lilensten et al. 2005). It consists of the computation of both primary production due to photoabsorption, and secondary production due to electron impact. A model of the Venusian thermosphere is required to achieve this computation. In the following, we describe how the code was developed to compute the excitation and emission rates.

2.1. Overview of the code

The main function of the TRANS-VENUS code is to compute the production of ions and excited species. By adding a chemical model, the densities and emissions of these species can be derived (see paragraph 3). The inputs are a neutral atmosphere model, an EUV/XUV flux model, and an electron precipitation spectrum for the nightside. A model of electron and ion densities and temperatures is required because the TRANS-VENUS code to date includes no fluid part. All of these models are described in the following section.

2.2. Adaptation of the code to Venus

The primary production is computed through a Beer-Lambert law (e.g. Simon et al. 2005). We use the semi-empirical model EUV/XUV called solar 2000 (Tobiska 1991, 1993; Tobiska & Eparvier 1998). In this model, the EUV spectrum is divided into 39 energy boxes, which correspond to wavelengths from 2 to 105 nm. These boxes are sufficient in the modelling of ionisation, but not of excitation mechanisms. We added a simple model for wavelengths ranging from 105 to 170 nm, which includes the Ly_α line (Bossy 1983). The dependence of the new

fluxes on solar activity, is implied by both the $F_{10.7}$ parameter (used in addition with the other fluxes), and the $F^{av}_{10.7}$ parameter (the three months average of $F_{10.7}$). The low-energy, UV solar lines (from Ly$_\alpha$, 1216 Å to 1800 Å) are necessary to compute the O(^{1}S) and O(^{1}D) states (upper states of the transitions that create the green 5577 Å line, and red triplet lines, about 6300 Å) from CO_2 photodissociation. The cross-section is adapted from Lawrence (1972b) and Slanger et al. (1974). However, large uncertainties about the differential cross section remain, and hence about the red line production rates (Huestis & Slanger 2006). The production of ions and excited states by photoelectron impact is computed using a multi-stream code (Lilensten & Blelly 2002; Simon et al. 2005). The major modifications with regards to the Martian and Titan models (Witasse 2000; Lilensten et al. 2005) concern the atmospheric model (thermosphere, ionosphere with electron and ion temperatures, and the electron density), and the excitation cross-sections, some of which have been added to the Martian model. The neutral atmosphere is computed from the VTS3 model (Hedin et al. 1983). The neutral species considered in the model are CO_2, N_2, CO, O, H, and N. At all altitudes, the O_2 concentration is considered to be 3×10^{-3} that of CO_2 (Fox & Sung 2001). Taking the altitude density profile of H atoms provided by Hartle et al. (1996), even if both H and N atoms are considered for chemical reactions, their ionisation is not accounted for, because the H^+ and N^+ ionised species do not contribute significantly to the emission (Fox & Sung 2001).

Observations of solar activity, location, time, and solar zenith angle, are used as input conditions for the VTS3 model. The neutral temperature is taken from the VTS3 model, the ion temperature is based on Fox & Sung (2001), and the electron temperature is taken from Theis et al. (1980, 1984), extended down to 100 km in correlation with Fox and Sung's temperature. It allows extending the model applicability to nighttime conditions. An example of temperatures can be found in Fig. 1. The electron density is taken from Theis et al. (1980, 1984), and is based on PVO measurements. Because some excitations are caused by the recombination of ion species, an ion density model is required. CO($a^3\Pi$) can for example be excited by the recombination of CO_2^+. In addition, the densities of CO_2^+, and O_2^+ are needed. In preparation for VEX future data, we use a stationary chemical model ($\frac{dn}{dt} = 0$ with n a specie concentration, t, time). The reaction rates are taken from Fox & Sung (2001). Fox & Sung (2001) showed that the electron density is approximately equal to the O_2^+ density below 200 km, and to the O^+ density above this altitude. We adapted the code accordingly (see Fig. 1). In the future, the ion density model will be improved by the inclusion of a fluid transport module. The densities provided by the code are inaccurate, but sufficient to determine emission rates approximately, which is our main objective.

2.3. Cross section of the Venusian species

- CO_2 and CO: ionisation cross-sections (for both primary and secondary productions) were reviewed by Witasse (2000). Excitation (non-dissociative and dissociative) cross-sections are summarised in Tables 1 and 2.
- N_2: ionisation and excitation cross-sections are listed in Lilensten et al. (2005).
- O and O_2: ionisation and excitation cross-sections are listed in Lilensten & Blelly (2002). The cross-section for the $O(^3P)_{\text{ground state}}$ $_{(1s)^2(2s)^2(2p)^3(3s)^1}$ $-O(^3P)_{(1s)^2(2s)^2(2p)^3(3p)^1}$ transition by electron impact excitation is taken from Gulcicek et al. (1988).

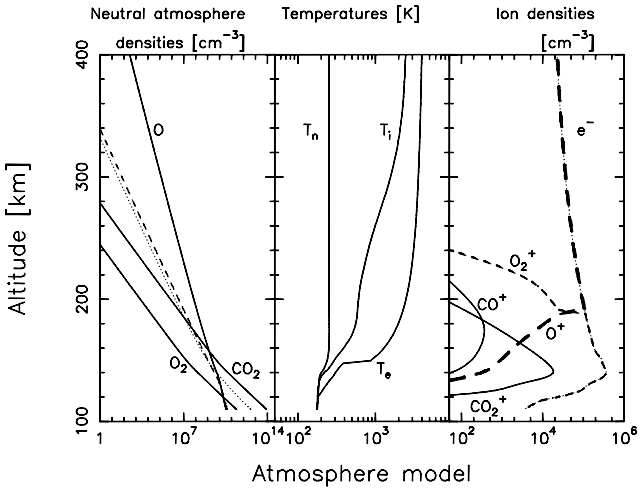

Fig. 1. The dayside upper atmosphere model. *In the left panel*, the dotted line represents the N_2 density and the dashed line the CO density. *In the center panel*, T_n is the neutral temperature, T_i the ion temperature, and T_e the electron temperature. *In the right panel*, an ion density semi-empirical model is used. This model was computed for $F_{10.7} = 80$, latitude: 45° at noon.

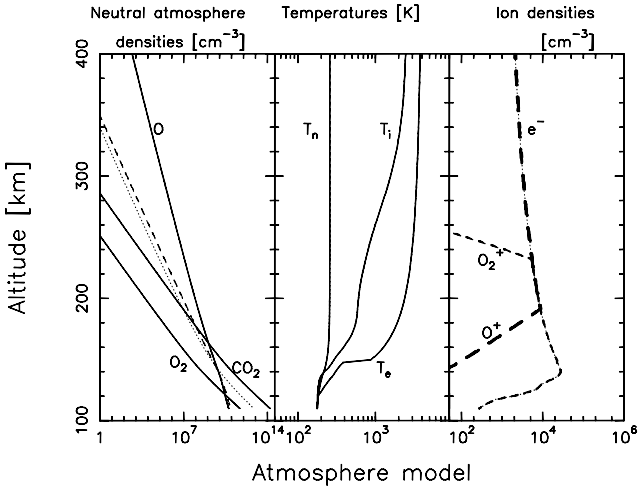

Fig. 2. The nightside upper atmosphere model. *In the left panel*, the dotted line represents the N_2 density and the dashed line the CO density. *In the center panel*, T_n is the neutral temperature, T_i the ion temperature, and T_e the electron temperature. *In the right panel*, an ion density semi-empirical model is used. This model was computed for $F_{10.7} = 80$, latitude: 0°, Solar zenith angle: 125°.

- O^+: ionisation cross-sections are summarised in Simon et al. (2005).

3. Modelling the emission lines

The dayglow spectrum of Mars and Venus, which are planets with an atmosphere mainly composed of CO_2, is dominated by the CO Cameron and Fourth Positive bands below 2700 Å (Leblanc et al. 2006; Fox & Bougher 1991). The other constituents of the spectrum are H, O and C lines, and some N_2 bands. Moreover, the CO_2^+ doublet can be seen at 2883–2896 Å. The nightglow spectrum of these planets consists mainly of O_2 and NO emissions (Fox & Bougher 1991), although other lines and bands are visible.

Table 1. Excitation cross section sources for the Cameron bands and the Fourth Positive bands of CO.

Specie/process	$CO(a^3\Pi)$ Cameron Bands 1900–2700 Å	$CO(A^1\Pi)$ 4th Positive bands 1200–1800 Å
CO_2		
Photodissociation	Lawrence (1972a)	Gentieu & Mentall (1972)
Electron impact	Witasse (2000)	Ajello (1971b)
$CO_2^+ + e^-$	Skrzypkowki et al. (1998)	Tsuji et al. (1998)
CO		
Resonant scattering	James (1971)	Eidelsberg et al. (1999)
Electron impact	Ajello (1971a)	Beegle et al. (1999)

Table 2. Excitation cross section sources for atomic oxygen emissions.

Specie/process	$O(^1S)$ Green line 5577 Å Forbidden transition	$O(^1D)$ Red line 6300 Å Forbidden transition	$O(^3S)$ 1304 Å	$O(^5S)$ 1356 Å
CO_2				
Photodissociation	Lawrence (1972b)	Slanger et al. (1974)	Wu & Judge (1979)	
Electron impact	Witasse (2000)		Ajello (1971b)	Ajello (1971b)
CO				
Photodissociation			Wu & Judge (1979)	
Electron impact			Ajello (1971a)	
O				
Resonant scattering	ng[1]	ng	Biemont & Zeippen (1992)	Biemont & Zeippen (1992)
Electron impact	ll94[2]	ll94	ll94	ll94

[1] Negligible.
[2] Lummerzheim & Lilensten (1994).

To model the emission lines and bands, we must compute the densities of excited states, which can be populated by electron impact excitation or dissociation (by recombination, photoabsorption or electron impact) of a molecule, and by resonant or fluorescent scattering.

- Resonant scattering is the production of an excited state by photoexcitation, followed by radiative relaxation; photons are both emitted and absorbed at the same wavelength. The $O(^3S) \rightarrow O(^3P)$ transition, for example, emits a line at 1304 Å. The resonant scattering that produces the $O(^3S)$ state is thus the excitation of $O(^3P)$ at 1304 Å which produces $O(^3S)$.
  Resonant scattering is important when solar lines are present at these wavelengths. Resonant scattering is normally described by a radiative-transfer model.
- Fluorescent scattering is similar to resonant scattering (excitation by photoabsorption) but produces the emission of bands instead of lines: the excited state can be populated by wavelengths that can be very different. The Fourth Positive bands can for example be populated by the Ly_α line, and by the 1304 Å line (even if the second case is negligible in practice).
- Loss rates such as quenching, and relaxation by emission, are required to compute the density. We therefore require the quenching rates and the Einstein factors A.

The quenching for allowed transitions are negligible, but not those of forbidden transitions that have a long deactivation time (small Einstein A factor). More precisely, the Einstein factor for spontaneous emission should be greater than the collision frequency. The collision frequency is approximately 10^3 s^{-1} at 100 km (the basis of our altitude grid), and decreases with increasing altitudes to values about 1 at 400 km. Resonant scattering is not negligible for allowed transitions. A radiative transfer code is therefore required to model the lines on the dayside. Since our radiative transfer model is still in development, we will not address resonant scattering. A band is the result of many rovibronic deactivations, and to compute a line (of this band) is equivalent to analysing one of its states. The Einstein coefficient of this particular transition and hypothesis (or data) on the vibrational and rotational temperatures, are required to know the state populations.

3.1. O

The relaxation of atomic oxygen in various states produces four main features (lines, multiplets) in the planetary dayglow and nightglow: the red line (a triplet), the green line (with a proportional multiplet at 2976 Å), and the 1304 and 1356 Å multiplet (Fig. 3).

3.1.1. Green line: $O(^1S) \rightarrow O(^1D)$ and 2972 Å multiplet: $O(^1S) \rightarrow O(^3P)$

The deactivation of the $O(^1S)$ oxygen state, creates the green line $O(^1S) \rightarrow O(^1D)$ at 5577 Å, and the 2972 Å emission ($O(^1S) \rightarrow O(^3P)$). The branching ratio is 94% for the green line, and 6% for

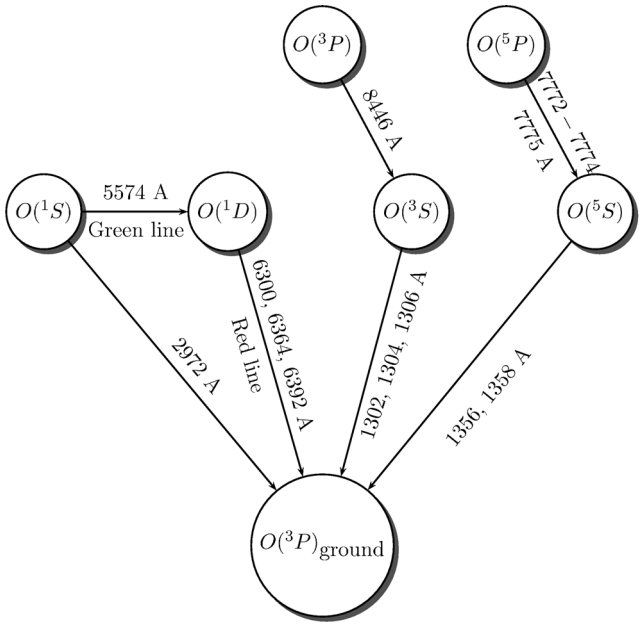

Fig. 3. States and transitions of atomic oxygen taken into account. Except for $O(^5P)$.

2972 Å. This is the recommended NIST $I(5577)/I(2972) = 16$ value. Slanger et al. (2006a) report a ratio of 9.8 ± 1.0 for the terrestrial nightglow, which is not used in this article. Because both transitions are forbidden, the state is metastable and we have to compute the quenching factors.

Production mechanisms of the $O(^1S)$ state:

- p1: electron-impact on O;
- p2: dissociative recombination of O_2^+;
- p3: collisional deactivation of $N_2(A^3\Sigma_u^+)$;
- p4: O_2 photodissociation;
- p5: barth mechanism (or alternative reaction: $N + O_2^+$, see below and Appendix A);
- p6: CO_2 photodissociation;
- p7: electron-impact on CO_2.

Loss mechanisms:

- l1: radiative transitions (to $O(^1D)$ and $O(^3P)$);
- l2: quenching by O_2;
- l3: quenching by O;
- l4: quenching by CO;
- l5: quenching by CO_2;
- l6: quenching by N_2;
- l7: quenching by electron-impact.

The above quenching reactions mainly relax the $O(^1S)$ state to the ground state ($O(^3P)$), but can also produce $O(^1D)$. Reaction rates are given in Table 4. 31% of the O_2 quenching, and 63% of the CO_2 quenching, create the $O(^1D)$ state. The reaction $O(^1S) + e^- \rightarrow O(^1D) + e^-$ (quenching by electron impact) has a rate of 8.5×10^{-9} cm^{-3} s^{-1} (Berrington & Burke 1981).

The collisional deactivation of $N_2(A^3\Sigma_u^+)$, to produce $O(^1D)$ (reaction p3), is computed using the following expression (Lummerzheim & Lilensten 1994, and references therein):

$$P_{O(^1D)} = 0.36\, P_{N_2(A^3\Sigma_u^+)} \Big/ \left(1 + \frac{0.38}{2.8 \times 10^{-11} \times [O]}\right)$$

where P_x is the production of the species x and [O] is the O density.

On Earth, the Barth mechanism (Barth & Hildebrandt 1961) is at the origin of the nightglow mesospheric, green-line emission. This mechanism is a three-body process, followed by an excitation transfer: $O + O + M \rightarrow O_2^* + M$; $O_2^* + O \rightarrow O_2 + O(^1S)$, where M is a mixture of molecular oxygen and nitrogen. This mechanism is probably also responsible for nightglow emission on Venus, where M is carbon dioxide (Fox 2004). Following (Slanger et al. 2006b), it is efficient however only if the excited state O_2^* is $O_2(c^1\Sigma_u^-, \nu \geq 2)$. This high-vibrational level has never been observed in the Venusian atmosphere. This may be due to the observational process whereby the c-state produces the Herzberg II emission during deexcitation. The $\nu \geq 2$ emission was not observed, which is why Slanger et al. (2006b) proposed an alternative process that involves the reaction of $O_2(c^1\Sigma_u^-, \nu = 0)$ with CO, to form $O(^1S)$. Neither the chemical rate of this reaction, nor the population of the $\nu = 0$ state of O_2, however, are known, and we consider this assumption no further in this paper.

The second point is that the green line is highly variable (see for example Figs. 2–4 in Slanger et al. 2006b). The Barth mechanism is efficient at low altitudes (typically about 105 km), where the atmosphere is stable and can hardly account for the emission variability.

Back in the 1970s, Frederick et al. (1976); Kopp et al. (1977) proposed a new reaction in the Earth's thermosphere: $N + O_2^+ \rightarrow NO^+ + O(^1S)$. This reaction could account for the emission variability at Venus. However, the atomic and chemical parameters make this reaction improbable theoretically.

These three reactions (Barth, Slanger and Frederick/Kopp) are discussed in detail in the Appendix A. In the following, we will compare the Barth and the Frederick/Kopp mechanisms.

3.1.2. Red line: $O(^1D) \rightarrow O(^3P)$

The red line, a triplet at 6300, 6363, and 6391 Å, is produced by the deactivation of the $O(^1D)$ state. This state is metastable and thus the computation of the quenching is required. The production mechanisms of the $O(^1D)$ state are:

- p1: electron-impact on O;
- p2: dissociative recombination of O_2^+;
- p3: O_2 photodissociation;
- p4: thermal electron impact on O;
- p5: cascading from $O(^1S)$ state;
- p6: $N(^2D) + O_2$;
- p7: $N^+ + O_2$;
- p8: dissociative recombination of CO^+;
- p9: quenching of the $O(^1S)$ state that produce $O(^1D)$;
- p10: CO_2 photodissociation.

The loss mechanisms are:

- l1: radiative transitions;
- l2: quenching by O_2;
- l3: quenching by O;
- l4: quenching by N_2;
- l5: quenching by thermal electrons;
- l6: quenching by CO_2;
- l7: quenching by CO.

3.1.3. 8446 Å: $O(^3P)$

The 8446 Å line corresponds to the $O(^3P) \rightarrow O(^3S)$ transition. The $O(^3P)$ level electronic configuration, $(1s)^2(2s)^2(2p)^3(3p)^1$,

which should not be confused with the $O(^3P)$ fundamental state, is only populated by electron impact ($O(^3P)_{\text{ground state}} \rightarrow O(^3P)$ is forbidden). This transition populates the $O(^3S)$ level.

The transition $O(^3P) \rightarrow O(^3S)$ has an Einstein coefficient $A = 3.22 \times 10^7$ s^{-1}, whereas the coefficient for $O(^3P) \rightarrow O(^5S)$ at 6726 Å is $A = 6.44 \times 10^2$ s^{-1}. We can therefore neglect the second transition, and consider the $O(^3P)$ state as a secondary source of $O(^3S)$.

3.1.4. 1302–1304–1306 Å triplet: $O(^3S)$

The $O(^3S)$ level is unstable ($A_{1302} = 3.41 \times 10^8$ s^{-1}). Moreover, the 1304 Å line is optically thick for Venus (Fox & Bougher 1991). Kassal (1975, 1976) showed that the (9, 0) Fourth Positive bands of CO, contaminate the $O(^3S)$ triplet. We need to develop a radiative-transfer code that simulates correctly both dayside and nightside.

3.1.5. 7772–7774–7775 Å triplet: $O(^5P)$

As for the 8446 Å, the triplet near 7772 Å is a transition between two excited levels: $O(^5P) \rightarrow O(^5S)$. The Einstein coefficient for the transition is $A = 3.69 \times 10^7$ s^{-1}. This state can be considered as a secondary source of $O(^5S)$. We do not include this source in our simulations.

3.1.6. 1356–1359 Å doublet: $O(^5S)$

The $O(^5S)$ level is also an unstable level ($A_{1355} = 4.20 \times 10^3$ s^{-1}): although the transition is forbidden, the radiative decay is faster than the quenching decay. The $O(^5S) \rightarrow O(^3P)$ transition needs a radiative-transfer model because the (14, 4) Fourth Positive bands of CO contaminate the 1356 Å line (Kassal 1975, 1976). Moreover, the (3, 0) Lyman-Birge-Hopfield (LBH) bands at 1354 Å blend the line.

3.2. CO

The Cameron and Fourth Positive bands of CO, are the major features in the dayglow spectrum of Venus and Mars. These bands emit between 1200 and 2800 Å.

3.2.1. Cameron bands

The Cameron bands are intense between 1900 and 2700 Å. They are generated by the $CO(a^3\Pi) \rightarrow CO(X^1\Sigma)$ transition. Fluorescent scattering is negligible, and it is a metastable state (lifetime 8 ms, Fox & Bougher (1991) and references therein). We therefore only consider deactivation radiation for this state.

The production sources taken into account are:

- p1: dissociation through electron impact on CO_2;
- p2: CO_2 photodissociation;
- p3: CO_2^+ dissociative recombination;
- p4: electron impact on CO;

This simulation is valid on both dayside and nightside.

3.2.2. Fourth positive bands

The Fourth Positive bands emit radiation of wavelengths between 1200 and 2800 Å, which is of particularly high intensity between 1300 and 1800 Å (Fox & Bougher 1991). This is produced by an allowed transition between $CO(A^1\Pi)$ and $CO(X^1\Sigma)$. 90% of the dayside production of the upper state comes from the fluorescent scattering of the Ly_α line by the $v' = 14$ progression (Fox & Bougher 1991; Kassal 1975, 1976). In our model, the fluorescent scattering has not yet been implemented, and our simulation is therefore only valid at night. The production sources taken into account are:

- p1: dissociation through electron impact on CO_2;
- p2: CO_2 photodissociation;
- p3: CO_2^+ dissociative recombination;
- p4: electron impact on CO.

3.3. CO_2

The CO_2 molecule has only a few UV-Visible emission lines, because it tends to dissociate or ionise at low energy (≈10 eV). Thus, the ultraviolet emission of CO_2 is produced mainly by its ion, CO_2^+. The main emissions of this ion are the UV doublet close to 2900 Å, and the Fox-Duffendack-Barker bands. Both transitions are allowed, and resonant scattering is not negligible.

3.3.1. $CO_2^+(B^2\Sigma_u^+)$ UV doublet

The 2883–2896 Å doublet is produced by the radiative deactivation of the $CO_2^+(B^2\Sigma_u^+)(0, 0, 0)$ state to the ground level. The resonant scattering of this transition is negligible (2% of the total production), considering electron impact ionisation or photoionisation of CO_2 (Fox & Bougher 1991).

3.3.2. $CO_2^+(A^1\Pi_u)$: the Fox-Duffendack-Barker bands

These bands arise from the radiative deactivation of the $CO_2^+(A^1\Pi_u)$ state to the ground level. Resonant scattering is responsible for 30% of this emission (Fox & Bougher 1991). The other sources are electron impact ionisation and photoionisation.

3.4. N_2

The N_2 emission lines have not yet been observed in the Venusian airglow.

As the atmosphere is composed of only 2% N_2, these lines (or bands) are expected to be weak. The detection of these emissions is therefore a challenging task for Venus Express.

3.4.1. $N_2(C^3\Pi_u - B^3\Pi_g)$ the Second Positive bands

The Second Positive bands come from the $N_2(C^3\Pi_u - B^3\Pi_g)$ allowed transition. Thus, it populates the $N_2(B^3\Pi_g)$ state, which is the upper state of the First Positive bands. The $N_2(C^3\Pi_u)$ state is populated by electron impact because the $N_2(C^3\Pi_u - X^1\Sigma_g^+)$ transition is forbidden. The Second Positive bands emit radiation in the 3200–3800 Å range.

3.4.2. $N_2(b'^3\Sigma_u - B^3\Pi_g)$ and $N_2(W'^3\Delta_u - B^3\Pi_g)$

As for the case of the Second Positive bands, these transitions are allowed. The upper states $N_2(b'^3\Sigma_u)$ and $N_2(W'^3\Delta_u)$, are populated only by electron impact.

3.4.3. $N_2(B^3\Pi_g - A^3\Sigma_u^+)$ the First Positive bands

The First Positive bands correspond to the $N_2(B^3\Pi_g - A^3\Sigma_u^+)$ allowed transition. They emit in the 6000–7500 Å range. In contrast to the $N_2(b'^3\Sigma_u - B^3\Pi_g)$ and $N_2(W'^3\Delta_u - B^3\Pi_g)$ transitions, the First-Positive-bands, upper-state is populated not only by electron impact, but also by cascade from more energetic states, and resonant scattering of the metastable, $N_2(A^3\Sigma_u^+)$-state.

3.4.4. $N_2(A^3\Sigma_u^+)$ the Vegard Kaplan system

The Vegard-Kaplan system is the $N_2(A^3\Sigma_u^+ - X^1\Sigma_g^+)$ transition. It emits in the 1500–6500 Å range. Because $N_2(A^3\Sigma_u^+)$ is metastable, the quenching processes have to be taken into account. Another effect is the photoexcitation of the $N_2(A^3\Sigma_u^+)$ state by photons. Since the First Positive bands transition is allowed, and its lower level is metastable, resonant scattering is possible (Broadfoot et al. 1997), but is not taken into account in our modelling. The Einstein factor is taken from Shemansky (1969). The quenching factors in cm^{-3} s^{-1} are 3.1×10^{-11} for oxygen, 4.1×10^{-12} for O_2, $1. \times 10^{-14}$ for CO_2, and $2. \times 10^{-11}$ for CO (Dreyer et al. 1974).

3.4.5. $N_2(a^1\Pi_g - X^1\Sigma_g^+)$ the Lyman-Birge-Hopfield system

The Lyman-Birge-Hopfield (LBH) system is populated through electron impact excitation. It emits in the 1273–2190 Å range.

3.4.6. $N_2(b^1\Pi_g - X^1\Sigma_g^+)$ the Birge-Hopfield system

The Birge-Hopfield (BH) system is populated through electron impact excitation. It emits in the 950–1700 Å range.

3.4.7. $N_2^+(B^2\Sigma_u^+ - X^2\Sigma_g^+)$ the First Negative bands

The First Negative bands emit mainly at 3991 and 4278 Å, in the 0–0 and 0–1 bands. It originates in an allowed ion transition.

The sources are electron impact ionisation, photoionisation, and fluorescent scattering. At the present stage, our model only takes into account the electron impact ionisation, thus being applicable only to the nightside.

3.4.8. $N_2^+(A^2\Sigma_u^+ - X^2\Sigma_g^+)$ the Meinel bands

The Meinel bands emit in the range 6400–8000 Å. As for the First Negative bands, photoionisation and fluorescent scattering have to be taken into account for dayglow modelling. The model presently computes its nightglow.

3.5. O_2 and NO spectrum

Previous observations of the Venus nightglow emissions have shown that O_2 Herzberg II bands and NO γ and δ bands, are major features of this spectrum (Fox & Bougher 1991). Some mesospheric chemical reaction also excite O_2 (Slanger 1978; Lawrence et al. 1977; Fox & Bougher 1991; Slanger et al. 2006b; Huestis & Slanger 1993). These reactions are mainly recombination processes, involving two or three bodies, such as the $O + O + CO_2 \rightarrow O_2^* + CO_2$ reaction, for which O is transported from the dayside, where it is produced by dissociation of CO_2.

Other mesospheric chemical reactions produce the NO bands, mainly through recombination processes of atomic nitrogen with atomic oxygen (Fox & Bougher 1991; Huestis & Slanger 1993).

The altitude of the maximum production of both O_2 and NO bands, is approximately 100 km, which is beneath the ionosphere. Moreover, mesospheric chemistry is required, preventing us from including such productions in our model.

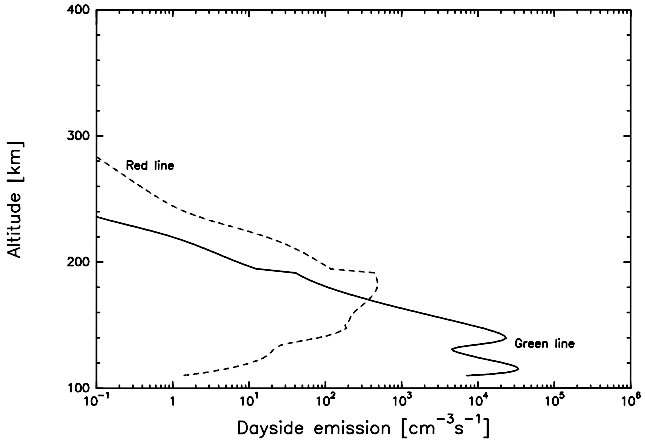

Fig. 4. The red and green line dayside emission profiles.

4. Dayside results

In the following paragraphs, all values will be expressed in units of Rayleigh, which is the emission of 10^6 photons in all directions, by a source column of 1 cm^2 section. For our simulations, this column is orientated toward nadir. We count the population of a state in a column, in addition in Rayleigh. For these cases, the Rayleigh unit is the column integration of the state density, divided by 10^6.

4.1. Atomic oxygen

4.1.1. Green line ($O(^1S)$ state)

The green line was observed indirectly, by Pioneer Venus Orbiter, at 2972 Å (Huestis & Slanger 1993). Lecompte et al. (1989) report an observation of 7 kR emission on orbit 187 ($F_{10.7} \approx 180$, $F_{10.7}^{av} \approx 160$, latitude = 45°, noon). For the same conditions, our simulation shows an intensity of 6.6 kR, in good agreement with the measurement. For that simulation, we find that about 85% of the dayside excitation is produced by the CO_2 photodissociation. In contrast, the O_2 photodissociation produces 2×10^{-5} times less $O(^1S)$, 8% from CO_2 electron impact dissociation, 2% from O_2^+ dissociative recombination, 1% from O electron impact excitation, and 1% from $N_2(A^3\Sigma_u^+)$ deactivation by O.

For a smaller solar activity ($F_{10.7} = 80$, latitude = 45°, noon), a value of 71 kR is computed for the green line, and 4.4 kR for the 2972 Å line (see Fig. 4).

Both the Barth and Frederick/Kopp processes, described in the Appendix, are negligible on the dayside. Their effect on overall emission is approximately a few hundreds Rayleighs.

4.1.2. Red line ($O(^1D)$ state)

There is no report of red line observations on the dayside of Venus. Our simulation shows a red line intensity of 2 kR for low solar activity ($F_{10.7} = 80$). 86.5% of the excitation

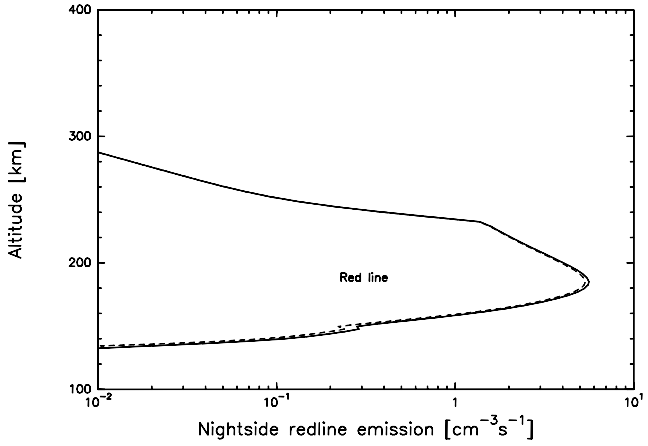

Fig. 5. The red line nightside emission profile. Dashed line: without the $O_2^+ + N$ reaction. Full line: with it. The influence of the Barth process is not shown because the quenching of the $O(^1D)$ state is too important at these altitudes. The main point in this simulation is that the observation of the red line cannot give evidences on the $O_2^+ + N$ reaction.

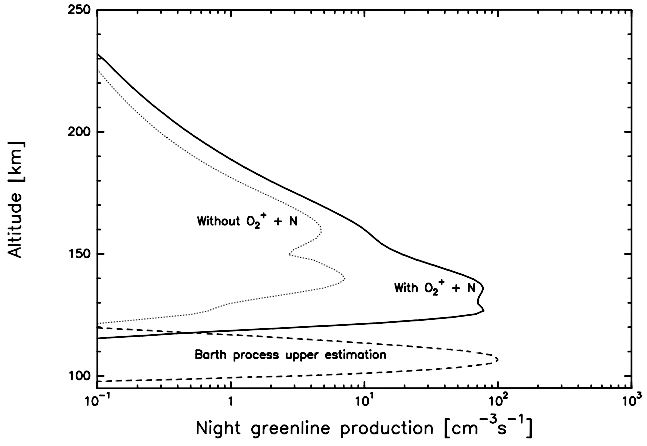

Fig. 6. Production of the nightside green line considering different chemical reactions $F_{10.7} = 80$, latitude: 0°, SZA: 125°.

originates from CO_2 photodissociation, 9% from O_2 photodissociation, 2.5% from $O(^1S)$ deactivation, and 2% from the electron impact on O_2 (and O) (see Fig. 4). Such an emission should be detectable using a spectrometer from Earth, which would produce a more accurate measurement of the $O(^1D)$ yield from the photodissociation of CO_2.

4.2. Allowed transitions

The simulation shows a 8446 Å emission at 300 R (Fig. 7), which is almost one third of the $O(^3S)$ non-radiative excitation (1.1 kR). The other main source of $O(^3S)$ is electron impact on O (775 R). For $O(^5S)$, although not allowed, (see Sect. 3.1.6), the excitation by electron impact on O, is 321 R, while the electron impact dissociation of CO_2, creates 22 R. The production of the state that does not come from resonant scattering, is thus 343 R.

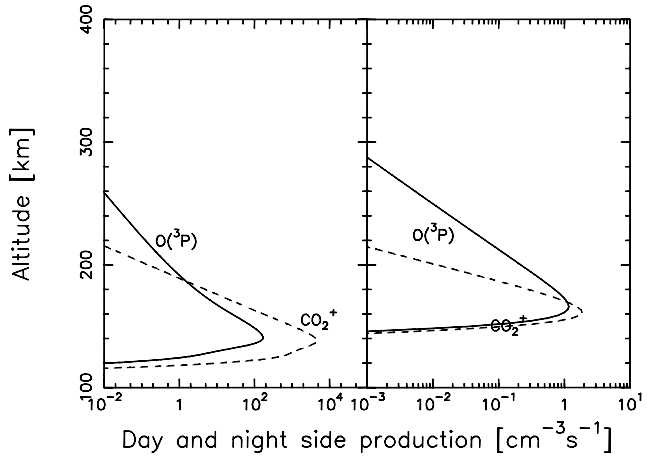

Fig. 7. The 8446 Å $O(^3P)$ and the $CO_2^+(B^2\Sigma_u^+)$ doublet line emission profiles. *Left panel*: dayside emissions. *Right panel*: nightside emissions.

4.3. Carbon monoxide and dioxide

4.3.1. Cameron bands

The Cameron-bands emission altitude profile, can be found in Fig. 8. On the dayside, the intensity is 17.3 kR, 7 kR originating from electron impact on CO_2, 5.3 kR from CO_2 photodissociation, 4 kR from electron impact on CO, and 1 kR from CO_2^+ dissociative recombination.

4.3.2. Fourth Positive bands

The Fourth Positive bands production, not arising from fluorescent scattering, has an intensity of 676 R: 220 R from electron impact on CO, 212 R from CO_2 photodissociation, 160 R from CO_2^+ dissociative recombination, and 84 R from electron impact on CO_2.

4.3.3. CO_2^+ doublet

The dayside intensity of the CO_2^+ doublet is 6.9 kR. The emission profile can be found in Fig. 7.

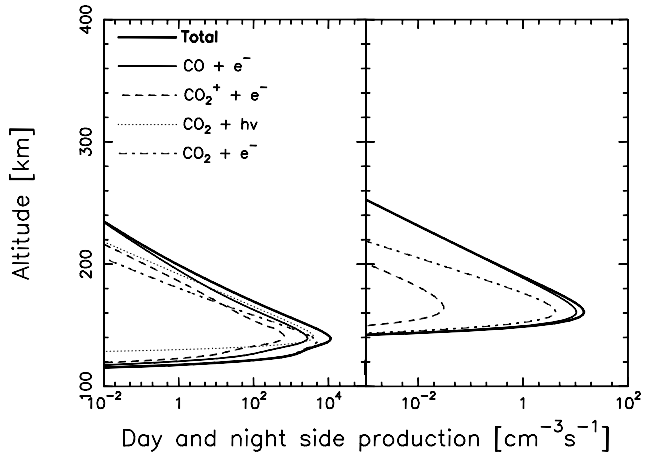

Fig. 8. Cameron bands system emission profiles. *Left panel*: dayside emissions. *Right panel*: nightside emissions. The influence of each sources is plotted.

4.4. Molecular nitrogen

The Second and First Positive N_2 bands, have intensities of 760 R and 1650 R, respectively. The Vegard Kaplan bands, have a non-radiative production of 310 R. The LBH bands have a production of 1.5 kR, from which 91 R are emitted at 1354 Å,

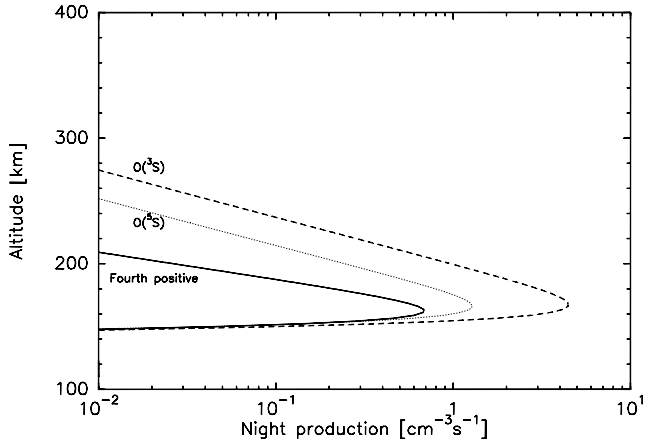

Fig. 9. Fourth Positive bands system emission profile and O(^{3}S) and O(^{5}S) production profile at night.

overlapping with the 1356 Å atomic oxygen line. The BH bands have a total integrated emission of 310 R.

We computed an electron impact production of 134 R for the 3914 Å line, 42 R for the 4278 Å line, and 740 R for the Meinel bands, all for the N_2^+ emissions, which require fluorescent scattering and photoionisation.

5. Nightside results

As opposed to the dayside, modelling the nightside of Venus' ionosphere requires external inputs that are difficult to estimate. For the dayside, the UV flux can be derived from direct observations (e.g. the observation at Earth, through the $F_{10.7}$ proxy, can be used). On the nightside, the energy input is electron precipitation. Owing to the lack of in-situ measurements, we can only estimate such a precipitation, which can be strongly variable, because it comes from the interaction between the planet and the highly-variable solar wind. For our calculations, we used the electron energy spectrum from Spenner et al. (1996).

5.1. Oxygen

5.1.1. Green line

In the mid seventies, the Venera probe did not observe any green line nightglow emission, during low solar activity. An upper value of 10 R was therefore proposed in Krasnopolskii (1981). The discovery of the green line, using the Keck telescope was made during moderate solar conditions. Slanger et al. (2001) report a nightime zenith intensity of 150 R. In order to reproduce this observation, we test two different reactions, wich we discuss in detail in the Appendix A. The standard mechanism is the Barth reaction. In Fig. 6, we show our computation for a solar zenith angle of 125°. This mechanism is efficient at approximately 105 km. The O(^{1}S) production reaches a value of about 100 cm^{-3} s^{-1}, resulting in an integrated green-line emission of 90 R, which is not far from observation. This result is obtained with a set of chemical reaction rates, based on the similarity beween CO_2 and O_2 as quenchers. Another choice of parameters (quenching ratio) can easily result in an emission intensity of 150 R (see Appendix A). In the same figure, we show the results of the O(^{1}S) production due to the alternative Frederick/Kopp mechanism $O_2^+ + N$. This reaction requires O_2^+ densities (Singhal 1996). The O(^{1}S) production due to Frederick/Kopp's reaction peaks at higher values than that of the Barth mechanism, between 130 and 140 km altitude. With this reaction, the integrated green-line emission is again comparable to observations, 150 R.

Without taking into account any of these mechanisms, we obtain an integrated green-line emission, of 21 R, which is much too small compared to observations.

Regarding the physico-chemistry, the Barth mechanism is the most probable. However, large uncertainties remain, which are explained in the Appendix A. The Frederick/Kopp reaction, although chemically possible, is difficult to achieve, because the internal energy available in the $O_2^+ + N$ reaction (4.3 eV), is close to the O(^{1}S) energy (4.2 eV). In the future, it will be necessary to explore in detail this latter reaction, and to make in-situ or limb observations of the oxygen green-line, to determine the altitude of its peak intensity, and to discriminate between the two reactions.

One additional issue will be to explain the high variability of the green-line emission. As observed by the Keck telescope, the emission varies from a deci-Rayleigh (lower detection limit) to an upper limit, which was probably more than the 167 R in its initial detection (Slanger et al. 2006b). How mesospheric processes can explain such a variability is still a debated question (see Appendix A). In contrast, PVO observations (`http://pds-ppi.igpp.ucla.edu/pvoven.htm`) show an O_2^+ variability of one order of magnitude or more, which could be compatible with the variability of the green-line emissions. The model shows that the Barth and/or Frederick/Kopp mechanisms (or a third one, see Appendix A) are responsible for the major part of the green nightglow emission. To a smaller extent, the O(^{1}S) states are also populated by other processes, namely dissociative recombination of O_2^+, electron impact on CO_2, and electron impact on O, in decreasing order of importance.

5.1.2. Red line

The nightside simulation shows a red-line intensity of 27 R at 6300 Å (in the same conditions as the green-line simulations). In spite of a 30% difference, this result is compatible with the observations of Slanger et al. (2001), who estimated an upper value of 20 R. The overestimate may be attributed to the bad constraints regarding O_2^+ densities. Because the intensity is low, our value is nonetheless in the observation error range. 55% of the excitation comes from the O_2^+ dissociative recombination, 35% from O(^{1}S) deactivation (quenching and radiative transition), and 10% from electron impact on O.

5.1.3. Allowed transitions

At night, the atomic-oxygen, allowed-transitions are weak: 4 R for the 8446 Å line, 14 R for the O(^{3}S) excitation (10 R from electron impact on O, 4 R from the O(^{3}P) deactivation). The 4 R production of O(^{5}S) (though not allowed, see Sect. 3.1.6) originates from electron impact on O.

We consider that the 1304 Å emission of the O(^{3}S) excited state is optically thick on the nightside. In that case, the 1304 Å emission is about 5 R. This is compatible with observations that derive an average value of 10 R (Fox & Bougher 1991), and, considering the sources of the line, it is compatible with the assumption of a soft electron source. This last hypothesis is compatible with the observation of the variability of the line, because the soft electron spectrum is very variable (Spenner et al. 1996). However, this will have to be studied in detail using a radiative transfer model.

Table 3. The emitting species in the Venusian atmosphere. The dayside modelling is done for $F_{10.7}$ = 80, lat = 45°, noon. Nightside emission calculations are based on the electron precipitation spectrum by Spenner et al. (1996).

Species	Transition	Wavelength	Observed	Observations (importance, fluorescent scattering, our prediction)
CO_2^+	$CO_2^+(B^2\Sigma_u^+)$	UV doublet (2883, 2896 Å)	No?[3]	Estimated at 10 kR, observed at Mars, fluorescence quasi-negligible (5%). Our model: dayside: 6.9 kR nightside: 3.38 R
	$CO_2^+(A^2\Pi_u)$	Fox-Duffendack-Barker bands (2800–5000 Å)	No?	Estimated at 15 kR, Observed at Mars, Fluorescence: 30% (Fox & Dalgarno 1981). Our model: dayside: 19.5 kR (without fluorescence) nightside: 13.5 R
CO	$CO(a^3\Pi)$	Cameron bands (1900–2700 Å)	Stewart et al. (1979)	Fluorescent scattering negligible Our model: dayside: 17.3 kR nightside: 30 R
	$CO(A^1\Pi)$	Fourth Positive bands (1200–2800 Å)	Dayside: Feldman et al. (2000)	Fluorescent scattering important Contaminates O 1304, 1356 Å lines. Our model: dayside: 680 R without fluorescent scattering nightside: 1.5 R
	$CO(C^1\Sigma^+)$	Hopfield Birge bands ((0, 0) at 1088 Å)	Dayside: Feldman et al. (2000)	Observation: 44 ± 6R ($CO(C^1\Sigma^+)(0,0)$) Not in our model.
	$CO(B^1\Sigma^+)$	Hopfield Birge bands ((0, 0) at 1152 Å)	Dayside: Feldman et al. (2000)	Observation : 128 ± 10R ($CO(C^1\Sigma^+)(0, 0)$) bundled with oxygen at 1151 Å Not in our model.
O	$O(^1S)$	Green line 5577 Å, 2972 Å	Yes Night: Slanger et al. (2001) Day: Lecompte et al. (1989)	In the night, this line has a variable intensity. Our model: dayside: 71 kR (2972 Å: 4.4 kR) nightside: 180 R
	$O(^1D)$	Red line 6300 Å, 6363 Å, 6391 Å	No?	Upper limit: ≈20 R (night) Our model: dayside: 2 kR nightside: 27 R
	$O(^3S)$	1302 Å,1304 Å, 1306 Å	Yes (day) Feldman et al. (2000)	Optically thick, contaminated by $CO(A^1\Pi)$ Our model (excitation without radiative transfer and scattering): dayside: 1.1 kR nightside: 14 R
	$O(^5S)$	1356 Å,1358 Å	Yes (day) Feldman et al. (2000)	Contaminated by $CO(A^1\Pi)$ Our model (excitation without radiative transfer): dayside: 340 R nightside: 4 R
	$O(^3P)$ $((1s)^2(2s)^2(2p)^3(3p)^1)$	8446 Å	No?	Cascading to $O(^3S)$ Our model: dayside: 300 R nightside: 3 R
	$O(^5P)$	7772–7774–7775 Å	No?	Cascading to $O(^5S)$
	$O(^3D)$	989 Å	Yes (day) Feldman et al. (2000)	Observation: 45 ± 33 R Not in our model
	$O(^3S)$ $((1s)^2(2s)^2(2p)^3(4s)^1)$	1040 Å	Yes (day) Feldman et al. (2000)	Observation: 21 ± 7R Not in our model
	$O(^1D^0-{}^1D)$	1152 Å	Yes (day)	Observation 100 ± 14R contaminated

Table 3. continued.

Species	Transition	Wavelength	Observed	Observations (importance, fluorescent scattering, our prediction)
			Feldman et al. (2000)	by CO($B^1\Sigma^+$)(0, 0) at 1152 Å Not in our model
	$O^+(^4S^0)$	834 Å	Yes (day) Feldman et al. (2000)	Observation: 91 ± 41R Not in our model
N_2	$N_2(C^3\Pi_u - B^3\Pi_g)$	2nd Positive bands 3200−3800 Å	No	Transitions in Benesch et al. (1966) Our model: dayside: 760 R nightside: 1.8 R
	$N_2(b'^3\Sigma_u - B^3\Pi_g)$		No	
	$N_2(W'^3\Delta_u - B^3\Pi_g)$	17 000−34 000 Å	No	
	$N_2(B^3\Pi_g - A^3\Sigma_u^+)$	1st Positive bands 6000−7500 Å	No	Transitions in Benesch et al. (1966) Fluorescence scattering needed Our model: dayside: 1.6 kR (without fluorescent scattering) nightside: 3.8 R
	$N_2(A^3\Sigma_u^+ - X^1\Sigma_g^+)$	Vegard Kaplan 1500−6500 Å	No	Metastable state (2 s) Can be excited to an upper level by resonant scattering (not in our model) Our model: dayside: 310 kR nightside: 0.9 R
	$N_2(a^1\Pi_g - X^1\Sigma_g^+)$	Lyman Birge Hopfield 1273−2190 Å	No	Blend the 1356 Å line. Our model: dayside:1.5 kR Transition at 1354 Å: 91 R nightside: 3.6 R
	$N_2(b^1\Pi_g - X^1\Sigma_g^+)$	Birge Hopfield 950−1700 Å	No	Our model: dayside: 310 R nightside: 0.9 R
	$N_2^+(B^2\Sigma_u^+ - X^2\Sigma_g^+)$	First negative (0, 0) at 3991 Å	No	Photoionisation and fluorescent scattering are needed. (not in our model) Our model: dayside 3914 Å: 134 R 4278 Å =: 42 R Nightside: 0 R for both
	$N_2^+(A^2\Pi_u - X^2\Sigma_g^+)$	Meinel 7800−15300 Å	No	Photoionisation and fluorescent scattering are needed, but not in our model Our model: dayside: 740 R nightside: 0 R
N	$N(^2p^4\ ^4P)$	1134 Å	Yes (day) Feldman et al. (2000)	Observation : 35 ± 11 R Not in our model
	$N(^4s^4P)$	1200 Å	Yes (day) Feldman et al. (2000)	Observation: 77 ± 16 R Not in our model
O_2	$O_2(b^1\Sigma_g^+)$	Infrared	Yes (night) Parisot (1986)	Needs mesospheric chemistry (<200 R)
	$O_2(a^1\Delta_g)$	1.27 μm	Yes (night) Parisot (1986)	Bands at 1.27 μm most intense feature (1.2−1.5 MR) Needs mesospheric chemistry
	$O_2(A^3\Sigma_u^+)$	Herzberg I	Yes (night) Parisot (1986)	140 R
	$O_2(c^1\Sigma_u^-)$	Herzberg II	Yes (night) Fox & Bougher (1991)	2.7 kR (night), strongest feature)

Table 3. continued.

Species	Transition	Wavelength	Observed	Observations (importance, fluorescent scattering, our prediction)
	$O_2(A'^3\Delta_u - a^1\Delta_g)$	Chamberlain	Yes (night) Parisot (1986)	200 R
	$O_2(c^1\Sigma_u^- - a^1\Delta_g)$	Slanger		
	$O_2^+(A^2\Pi_u)$	Second negative		Fluorescent scattering needed
	$O_2^+(b^4\Sigma_g^- - a^4\Pi_u)$	First negative		Very weak
C	$C(^3D^0)$	1561 Å	Yes (day) Feldman et al. (2000)	Observed: 800 ± 27 R Not in our model
	$C(^3P^0)$	1657 Å	Yes (day) Feldman et al. (2000)	Observed 1500 ± 50 R Not in our model
	$C^+(^2D)$	1335 Å	Yes (day) Feldman et al. (2000)	Blended with (9, 1) CO Fourth Positive bands
NO	$NO(C^2\Pi - X^2\Pi)$	δ bands	Yes (night) Fox & Bougher (1991)	Not in our model
	$NO(A^2\Sigma^+ - X^2\Pi)$	γ bands	Yes (night) Fox & Bougher (1991)	Not in our model

[3] Probably present, but not reported yet.

Table 4. References for reaction rates, T_e is the electron temperature, T_i is the ion temperature, and T_n is the neutral temperature.

Reaction	Rate ($cm^{-3}\ s^{-1}$)	Reference
$O_2^+ + e^- \rightarrow O(^1S) + e^-$	$T_e > 1200$ K: $3.69 \times 10^{-9} \left(\frac{1200}{T_e}\right)^{0.56}$ $T_e < 1200$ K: $9.75 \times 10^{-9} \left(\frac{300}{T_e}\right)^{0.7}$	Kella et al. (1997)
$N_2(A^3\Sigma_u^+) + O \rightarrow O(^1S) + N_2$	See text	
$N + O_2^+ \rightarrow O + NO^+$	1.8×10^{-10}	Goldan et al. (1966)
$N + O_2^+ \rightarrow O(^1S) + NO^+$	2.25×10^{-11}	Frederick et al. (1976); Kopp et al. (1977) Ref. in Witasse et al. (1999)
$O_2 + O(^1S) \rightarrow O_2 + O(^3P)$ or $O(^1D)$ (31%)	$4.4 \times 10^{-12} \times \exp -\frac{865}{T_n}$	Capetanakis et al. (1993)
$O + O(^1S) \rightarrow 2O$	2×10^{-14}	Ref. in Lummerzheim & Lilensten (1994)
$CO + O(^1S) \rightarrow O + CO$	$7.4 \times 10^{-14} \times \exp -\frac{961}{T_n}$	Capetanakis et al. (1993)
$CO_2 + O(^1S) \rightarrow CO_2 + O(^3P)$ or $O(^1D)$ (63%)	$3.21 \times 10^{-12} \times \exp -\frac{1327}{T_n}$	Capetanakis et al. (1993)
$N_2 + O(^1S) \rightarrow O + N_2$	5×10^{-17} (negligible)	Atkinson & Welge (1972)
$e^- + O(^1S) \rightarrow O + e^-$	$8.656 \times 10^{-9} \times \left(\frac{T_e}{300}\right)^{0.94}$	Berrington & Burke (1981)
$O_2^+ + e^- \rightarrow O(^1D)$	$T_e > 1200$ K: $8.199 \times 10^{-8} \times \left(\frac{1200}{T_e}\right)^{0.56}$ $T_e < 1200$ K: $2.1675 \times 10^{-7} \times \left(\frac{300}{T_e}\right)^{0.7}$	Kella et al. (1997)
$O + e^-$ (thermal electrons) $\rightarrow O(^1D) + e^-$	$0.596 \sqrt{T_e}\ (9329 + T_e)\ \exp \frac{-22756}{T_e}\ (51183 + T_e)^{-3}$	Mantas (1994)
$N(^2D) + O_2^+ \rightarrow O(^1D) + \cdots$	5×10^{-10}	Ref. in Lummerzheim & Lilensten (1994)
$N^+ + O_2 \rightarrow O(^1D) + \cdots$	1.4×10^{-10}	Ref. in Lummerzheim & Lilensten (1994)
$CO^+ + e^- \rightarrow C + O(^1D)$	$0.25 \times 10^{-7} \left(\frac{300}{T_e}\right)^{0.55}$	Rosén et al. (1998)
$O_2 + O(^1D) \rightarrow O_2 + O$	$2.9 \times 10^{-11} \exp \frac{67.5}{T_n}$	Atkinson et al. (1997)
$O + O(^1D) \rightarrow 2O$	$6.47 \times 10^{-12} \times \left(\frac{300}{T_e}\right)^{0.14}$	Jamieson et al. (1992)
$N_2 + O(^1D) \rightarrow N_2 + O$	$2 \times 10^{-11} \exp \frac{107.8}{T_n}$	Atkinson et al. (1997)
$e^- + O(^1D) \rightarrow O + e^-$	$2.87 \times 10^{-10} \left(\frac{T_e}{300}\right)^{0.91}$	Berrington & Burke (1981)
$CO_2 + O(^1D) \rightarrow CO_2 + O$	$6.8 \times 10^{-11} \exp \frac{117}{T_n}$	Streit et al. (1976)
$CO + O(^1D) \rightarrow CO + O$	3.6×10^{-11}	Schofield (1978)

5.2. Weak lines of CO, CO_2^+, and N_2

Our simulations show a total integrated intensity of 30 R for the Cameron CO bands, and 1 R for the Fourth Positive bands system of CO. As a consequence, it is presently not possible to observe these bands, a conclusion that is compatible with previous observations, showing no occurrence of these band systems in the Venus nightglow. Fox & Bougher (1991) interpreted this result as the consequence of a horizontal magnetic field. Although not incompatible with this interpretation, our simulations show that this assumption is not necessary to account for the current observations.

For the CO_2^+ doublet, a total intensity of 3.4 R was computed.

For N_2^+, the nightside intensity is less than 1 R. For N_2, the bands intensities are below 4 R (see Table 3).

6. Conclusions

The reliability of the TRANS-VENUS code, one of the first multi-stream codes to compute the Venusian airglow, has been proven by experiment, for several emission lines and bands. The results of the simulations suggest that several mechanisms can explain the observed intensity of the green-line in the nightside of Venus, namely the Barth, and the controversial Frederick/Kopp mechanisms. In this latter case, the variations of the O_2^+ density (Bauer et al. 1985; Miller & Whitten 1991) could also explain the observed intensity fluctuations. Coordinated measurements from orbiting spacecraft, and Earth-based observatories, of both O_2^+ density and green-line intensity, on the nightside ionosphere of Venus, are however necessary to confirm this hypothesis. The Venus Express (VEX) mission has been orbiting Venus since April 2006 and the SPICAV experiment should help obtain such results. The three observational ranges of SPICAV (UV: 1180–3200 Å, IR 7000–17 000 Å, and 22 000–42 000 Å) will provide results on atomic oxygen lines, carbon monoxide or nitrogen bands. Further computational improvements are planned, especially where fluorescent excitation and radiative transfer are required. Moreover, solution of the fluid equations, and in particular the ion densities, will place stronger constraints on the shape of the ion density profiles.

Acknowledgements. The authors thank Olivier Witasse (ESTEC, Netherlands), Roland Thissen (LPG, France) and Tom Slanger (SRI, USA) for helpful discussions. We warmly thank the referee who made very pertinent remarks which allowed us to improve our paper significantly.

References

Ajello, J. 1971a, J. Chem. Phys., 55, 3169
Ajello, J. 1971b, J. Chem. Phys., 55, 3158
Alcaraz, C., Nicolas, C., Thissen, R., Zabka, J., & Dutuit, O. 2004, J. Phys. Chem. A, 108, 9998
Atkinson, R., Baulch, D. L., Cox, R. A., et al. 1997, J. Phys. Chem. Ref. Data, 26, 521
Atkinson, R., & Welge, K. 1972, J. Chem. Phys., 57, 3689
Barth, C. A., & Hildebrandt, A. F. 1961, J. Geophys. Res., 66, 985
Bauer, S. J., Brace, L. M., Taylor, Jr., H. A., Breus, T. K., & Kliore, A. J. 1985, Adv. Space Res., 5, 233
Beegle, L. W., Ajello, J. M., James, G. K., Dziczek, D., & Alvarez, M. 1999, A&A, 347, 375
Benesch, W., Vanderslice, J. T., Tilford, S. G., & Wilkinson, P. G. 1966, ApJ, 144, 408
Berrington, K. A., & Burke, P. G. 1981, Planet. Space Sci., 29, 377
Biemont, E., & Zeippen, C. J. 1992, A&A, 265, 850
Bossy, L. 1983, Planet. Space Sci., 31, 977
Bougher, S. W., Rafkin, S., & Drossart, P. 2006, Planet. Space Sci., 54, 1371
Broadfoot, A. L., Hatfield, D. B., Anderson, E. R., et al. 1997, J. Geophys. Res., 102, 11567
Capetanakis, F. P., Sondermann, F., Hoeser, S., & Stuhl, F. 1993, J. Chem. Phys., 98, 7883
Chapman, S. 1931, Proc. Phys. Soc., 43, 483
Crisp, D., Meadows, V. S., Bézard, B., et al. 1996, J. Geophys. Res., 101, 4577
Dreyer, J., Perner, D., & Roy, C. 1974, J. Chem. Phys., 61, 3164
Eidelsberg, M., Jolly, A., Lemaire, J., et al. 1999, A&A, 346, 705
Feldman, P. D., Burgh, E. B., Durrance, S. T., & Davidsen, A. F. 2000, ApJ, 538, 395
Fox, J. L. 2004, Adv. Space Res., 33, 132
Fox, J. L. & Bougher, S. W. 1991, Space Sci. Rev., 55, 357
Fox, J. L., & Dalgarno, A. 1981, J. Geophys. Res., 86, 629
Fox, J. L., & Sung, K. Y. 2001, J. Geophys. Res., 106, 21305
Frederick, J. E., Rusch, D. W., Sharp, W. E., et al. 1976, J. Geophys. Res., 81, 3923
Gentieu, E., & Mentall, J. 1972, J. Chem. Phys., 58, 4803
Goldan, P., Schmeltekopf, A. L., Fehsenfeld, F. C., Schiff, H. I., & Ferguson, E. E. 1966, J. Chem. Phys., 44, 4095
Gronoff, G., Lilensten, J., Simon, C., et al. 2007, A&A, 465, 641
Gulcicek, E. E., Doering, J. P., & Vaughan, S. O. 1988, J. Geophys. Res., 93, 5885
Hartle, R. E., Donahue, T. M., Grebowsky, J. M., & Mayr, H. G. 1996, J. Geophys. Res., 101, 4525
Hedin, A. E., Niemann, H. B., Kasprzak, W. T., & Seiff, A. 1983, J. Geophys. Res., 88, 73
Hohmann, J., Müller, G., Schönnenbeck, G., & Stuhl, F. 1994, Chem. Phys. Lett., 217, 577
Huestis, D. L., & Slanger, T. G. 1993, J. Geophys. Res., 98, 10839
Huestis, D. L., & Slanger, T. G. 2006, in AAS/Division for Planetary Sciences Meeting Abstracts, 62.20
James, T. 1971, J. Chem. Phys., 55, 4118
Jamieson, M. J., Finch, M., Friedman, R. S., & Dalgarno, A. 1992, Planet. Space Sci., 40, 1719
Kassal, T. 1975, Applied Optics, 14, 1513
Kassal, T. 1976, J. Geophys. Res., 81, 1411
Katsumata, S., Shiromaru, H., Mitani, K., Iwata, S., & Kimura, K. 1982, Chem. Phys., 69, 423
Kella, D., Vejby-Christensen, L., Johnson, P., Pedersen, H., & Andersen, L. 1997, Science, 276, 1530
Kopp, J. P., Frederick, J. E., Rusch, D. W., & Victor, G. A. 1977, J. Geophys. Res., 82, 4715
Krasnopolskii, V. A. 1981, Planet. Space Sci., 29, 925
Langford, A. O., Bierbaum, V. M., & Leone, S. R. 1985, Planet. Space Sci., 33, 1225
Langford, A. O., Bierbaum, V. M., & Leone, S. R. 1986, J. Chem. Phys., 84, 2158
Lawrence, G. 1972a, J. Chem. Phys., 56, 3435
Lawrence, G. 1972b, J. Chem. Phys., 57, 5616
Lawrence, G. M., Barth, C. A., & Argabright, V. 1977, Science, 195, 573
Leblanc, F., Chaufray, J. Y., Lilensten, J., Witasse, O., & Bertaux, J.-L. 2006, J. Geophys. Res. (Planets), 111, 9
Lecompte, M. A., Paxton, L. J., & Stewart, A. I. F. 1989, J. Geophys. Res., 94, 208
Lilensten, J., & Blelly, P. L. 2002, J. Atmosph. Terrestr. Phys., 64, 775
Lilensten, J., Witasse, O., Simon, C., et al. 2005, Geophys. Res. Lett., 32, 3203
Lummerzheim, D., & Lilensten, J. 1994, Ann. Geophys., 12, 1039
Mantas, G. P. 1994, J. Geophys. Res., 99, 8993
Martin, L. R., Cohen, R. B., & Schatz, J. F. 1976, Chem. Phys. Lett., 41, 394
McDade, I. C., Murtagh, D. P., Greer, R. G. H., et al. 1986, Planet. Space Sci., 34, 789
Miller, K. L., & Whitten, R. C. 1991, Space Sci. Rev., 55, 165
Murtagh, D. P., Witt, G., Stegman, J., et al. 1990, Planet. Space Sci., 38, 43
Parisot, J.-P. 1986, Annales Geophysicae, 4, 481
Rosén, S., Peverall, R., Larsson, M., et al. 1998, Phys. Rev. A, 57, 4462
Schofield, K. 1978, J. Photochem, 9, 55
Scott, G. B. I., Fairley, D. A., Freeman, C. G., McEwan, M. J., & Anicich, V. G. 1998, J. Chem. Phys., 109, 9010
Shemansky, D. 1969, J. Chem. Phys., 51, 689
Simon, C., Lilensten, J., Dutuit, O., et al. 2005, Annales Geophysicae, 23, 781
Singhal, R. P. 1996, J. Geophys. Res., 101, 4565
Skrzypkowki, M., Gougousi, T., Johnsen, R., & Golde, M. 1998, J. Chem. Phys., 108, 8400
Slanger, T. G. 1978, Geophys. Res. Lett., 5, 947
Slanger, T. G., Cosby, P. C., Huestis, D. L., & Bida, T. A. 2001, Science, 291, 463

Slanger, T. G., Cosby, P. C., Sharpee, B. D., Minschwaner, K. R., & Siskind, D. E. 2006a, J. Geophys. Res. (Space Physics), 111, 12318
Slanger, T. G., Huestis, D. L., Cosby, P. C., Chanover, N. J., & Bida, T. A. 2006b, Icarus, 182, 1
Slanger, T. G., Sharpless, R. L., Black, G., & Filseth, S. V. 1974, J. Chem. Phys., 61, 5022
Smith, M. A., Bierbaum, V. M., & Leone, S. R. 1983, Chem. Phys. Lett., 94, 398
Spenner, K., Knudsen, W., & Lotze, W. 1996, J. Geophys. Res., 101, 4557
Steadman, J. A., & Thrush, B. A. 1994, J. Atmosph. Chem., 18, 301
Stewart, A. I., Anderson, D. E., Esposito, L. W., & Barth, C. A. 1979, Science, 203, 777
Streit, G. E., Howard, C. J., Schmeltekopf, A. L., Davidson, J. A., & Schiff, H. I. 1976, J. Chem. Phys., 65, 4761
Theis, R. F., Brace, L. H., & Mayr, H. G. 1980, J. Geophys. Res., 85, 7787
Theis, R. F., Brace, L. H., Elphic, R. C., & Mayr, H. G. 1984, J. Geophys. Res., 89, 1477
Tobiska, W. K. 1991, J. Atm. Terr. Phys., 53, 1005
Tobiska, W. K. 1993, J. Geophys. Res., 98, 18879
Tobiska, W. K., & Eparvier, F. G. 1998, Sol. Phys., 177, 147
Tsuji, M., Nakamura, M., Nishimura, Y., & Obase, H. 1998, J. Chem. Phys., 108, 8031
Witasse, O. 2000, Ph.D. thesis, UJF, France
Witasse, O., Lilensten, J., Lathuillère, C., & Blelly, P.-L. 1999, J. Geophys. Res., 104, 24639
Witasse, O., Dutuit, O., Lilensten, J., et al. 2002, Geophys. Res. Lett., 29, 104
Witasse, O., Dutuit, O., Lilensten, J., et al. 2003, Geophys. Res. Lett., 30, 12
Witt, G., Stegman, J., Solheim, B. H., & Llewellyn, E. J. 1979, Planet. Space Sci., 27, 341
Wu, C. Y. R., & Judge, D. L. 1979, Chem. Phys. Lett., 68, 495

Appendix A: Different mechanisms to explain the nightside green line intensity

A.1. The Barth process

A.1.1. Principle

The process suggested by Barth & Hildebrandt (1961) to explain the intensity of the green line is an improvement of the three O recombination process proposed by Chapman (1931). It can be written:

$$O(^3P) + O(^3P) + M \rightarrow O_2^* + M \quad \text{reaction rate: } k_{\text{barth}} \tag{A.1}$$

$$O_2^* + O(^3P) \rightarrow O(^1S) + O_2 \quad \text{reaction rate: } k_{^1S-O_2^*-O} \tag{A.2}$$

where k_{Barth} represents the reaction rate of the three-body reaction (the main reaction of the Barth process), and $k_{^1S-O_2^*-O}$ is the reaction rate of the production of $O(^1S)$, during the reaction between O_2^* and $O(^3P)$. O_2^* is usually called the precursor. The third element M, in Eq. (A.1), stabilizes the reaction complex. It is primarily N_2 and O_2 at Earth, and CO_2 at Venus. The chemical coefficient of the Barth mechanism does not depend on M because of its energetic role. (For examples and reaction rates, see Witt et al. 1979.)

A.1.2. The complete equation

In both Earth and Venus' mesospheres, only the Barth mechanism can be considered in the O_2^* production. Let k_{E-G} be the reaction rate of the quenching of a species E by a species G. For instance, the reaction rate $k_{O_2^*-O_2}$ represents the quenching of O_2^* by O_2. The related densities taking part in the Barth mechanism are given by:

$$[O_2^*] = \frac{k_{\text{Barth}}[O]^2[M]}{A_{O_2^*} + k_{O_2^*-O_2}[O_2] + k_{O_2^*-N_2}[N_2] + k_{O_2^*-O}[O]} \tag{A.3}$$

$$\left[O(^1S)\right] = \frac{k_{^1S-O_2^*-O}[O_2^*][O]}{A_{O^1S} + k_{O^1S-O_2}[O_2] + k_{O^1S-N_2}[N_2]}. \tag{A.4}$$

Where A_G is the Einstein coefficient of the radiative desexcitation of G. The $O(^1S)$ density becomes:

$$\left[O(^1S)\right] = \frac{k_{^1S-O_2^*-O}k_{\text{Barth}}[O]^3[M]}{\left(A_{O^1S} + k_{O^1S-O_2}[O_2] + k_{O^1S-N_2}[N_2]\right)\left(A_{O_2^*} + k_{O_2^*-O_2}[O_2] + k_{O_2^*-N_2}[N_2] + k_{O_2^*-O}[O]\right)}. \tag{A.5}$$

This may be re-written as:

$$\left[O(^1S)\right] = \frac{k_{\text{Barth}}[O]^3[M]}{\underbrace{\left(A_{O^1S} + k_{O^1S-O_2}[O_2] + k_{O^1S-N_2}[N_2]\right)}_{\text{Terms of } O(^1S) \text{ quenching}}\underbrace{\left(\frac{A_{O_2^*}}{k_{^1S-O_2^*-O}} + \frac{k_{O_2^*-O_2}}{k_{^1S-O_2^*-O}}[O_2] + \frac{k_{O_2^*-N_2}}{k_{^1S-O_2^*-O}}[N_2] + \frac{k_{O_2^*-O}}{k_{^1S-O_2^*-O}}[O]\right)}_{\text{Terms of } O_2^* \text{ quenching}}}. \tag{A.6}$$

Ratios between reaction rates appear in the terms of O_2^* quenching. Neither the rates nor the ratios are known. At Earth, these ratios were fitted through the observation of the green line. Several sets of values have been published in the literature (McDade et al. 1986; Murtagh et al. 1990).
Equation (A.6) can be easily used for Venus by adding the quenching by CO_2.

A.1.3. The case of the Earth

The fits achieved in (McDade et al. 1986; Murtagh et al. 1990) for the quenching terms (the ratios above) result in neglecting the spontaneous desexcitation, and the quenching by N_2, in comparison to the $k_{^1S-O_2^*-O}$ term. This is due to the fact that the oxygen is an open-shell molecule – such as CO_2 – with many energetic states, which is not the case for N_2. The simplified equation becomes:

$$\left[O(^1S)\right] = \frac{k_{\text{Barth}}\,[O]^3\,([N_2]+[O_2])}{\left(A_{^1S}+k_{^1S-O_2}[O_2]\right)\left(C'^{O_2}[O_2]+C'^{O}[O]\right)}. \tag{A.7}$$

In the papers above, the fitted value of the $C'^{O} = \frac{k_{O_2^*-O}}{k_{^1S-O_2^*-O}}$ factor is 211. Mathematically, the ratio represents the efficiency of the $O_2^* + O \rightarrow O_2 + O$ reaction, compared to the creation of $O(^1S)$ by O_2^* quenching. The $C'^{O_2} = \frac{k_{O_2^*-O_2}}{k_{^1S-O_2^*-O}}$ factor was fitted to 15. If we consider that the fitted values are representative of the efficiency of the reactions, we can give the relative efficiency of the O_2^* quenching reactions:

$$\frac{C'^{O_2}}{C'^{O}} = \frac{k_{O_2^*-O_2}}{k_{O_2^*-O}} = 7.1^{-2}. \tag{A.8}$$

A.1.4. The problem of the precursor excited state

On Earth, the fits corresponding to the Barth parameters, result in neglecting the quenching by N_2 compared to the one by O_2. In the Venusian atmosphere, both CO_2 and O_2 have to be considered. For example, the $O_2(b^1\Sigma_g^+)$ state is quenched by N_2 with a coefficient rate of 2.2×10^{-15} cm^{-3} s^{-1}, Martin et al. 1976, whereas it is quenched by CO_2 with a coefficient rate 200 times higher ($(4.4 \pm 0.2) \times 10^{-13}$ cm^{-3}s^{-1} (Hohmann et al. 1994)).

The quenching coefficient rate depend on the excitation state of the precursor O_2^*. This excited state must be metastable, and must be energetic enough to produce $O(^1S)$ through collision, i.e. with an energy larger than 4.16 eV. Therefore, the O_2^* excited states to be considered are:

- $O_2(A^3\Sigma_u^+)$: lifetime 0.16 s, energy 4.34 eV, emitting Herzberg *I* bands;
- $O_2(A'^3\Delta_u)$: lifetime 1 s, energy 4.26 eV emitting Herzberg III and Chamberlain bands;
- $O_2(c^1\Sigma_u^-, \nu \geq 2)$: lifetime 3.7 s, energy >4.16 eV (4.05 eV for the fundamental vibrational state), emitting Herzberg II bands.

Slanger et al. (2006b) supposed that the Barth emissions come from $O_2(c^1\Sigma_u^-, \nu \geq 2)$, which has not yet been observed in the Venusian atmosphere, but has been observed at Earth. Therefore, they concluded that the Barth process cannot be efficient for Venus, and proposed another mechanism discussed below.

For Steadman & Thrush (1994), the Barth emission comes from $O_2(A^3\Sigma_u^+, \nu = 6, 7)$ visible through the Herzberg I bands. Parisot (1986) observe that the emission of Herzberg I is three times more intense at Earth, than at Venus. The green line emission is then expected to be three times smaller in the Venusian atmosphere, than in the Earth one. This is not what is observed: Slanger et al. (2006b) report similar intensities on both planets. This can be explained if the vibrational states $\nu = 6, 7$ of the emitter, are not divided by the same factor of three, that is, the vibrational state intensities are not separated in Parisot (1986).

A.1.5. The Barth mechanism in the Venusian case

For Venus, Eq. (A.6) becomes:

$$\left[O(^1S)\right] = \frac{k_{\text{Barth}}[O]^3[CO_2]}{\underbrace{\left(A_{^1S}+k_{^1S-O_2}[O_2]+k_{^1S-CO_2}[CO_2]\right)}_{\text{Terms of O(}^1\text{S) quenching}}\underbrace{\left(\frac{A_{O_2^*}}{k_{^1S-O_2^*-O}}+\underbrace{\frac{k_{O_2^*-O_2}}{k_{^1S-O_2^*-O}}}_{C'^{O_2}}[O_2]+\underbrace{\frac{k_{O_2^*-CO2}}{k_{^1S-O_2^*-O}}}_{C'^{CO_2}}[CO_2]+\underbrace{\frac{k_{O_2^*-O}}{k_{^1S-O_2^*-O}}}_{C'^{O}}[O]\right)}_{\text{Terms of O}_2^* \text{ quenching}}}. \tag{A.9}$$

Below, the oxygen densities are taken from Bougher et al. (2006). Since the excitation state of the precursor O_2^* is unknown, alternative hypotheses are required.

If we consider only the quenching of O_2^* by O_2 (with a factor C of 15, as on Earth), and O (with a factor C of 211, as on Earth), and we neglect the quenching by CO_2, we obtain an emission of 2.1 kR. This is too large, and indicates that the quenching of O_2^* by CO_2 must be considered, although its ratio C is unknown. Since CO_2 is an open-shell molecule such as O_2, we use as a first approximation the same ratio $C = 15$. We then obtain:

$$\left[O(^1S)\right] = \frac{k_{\text{Barth}}\,[O]^3\,[CO_2]}{(A+k_{O1S-CO2}[CO_2])\left(C'^{CO_2}(=15)[CO_2]+C'^{O}(=211)[O]\right)}. \tag{A.10}$$

The result is shown in Fig. 6 and exhibits a peak emission at 90 R. This is in correct agreement with the observations (Slanger et al. 2006b). For better agreement, it is of course possible to fit C'^{CO_2} in order to retrieve the integrated intensity of 150 R. A value of 7 (instead of 15) gives an integrated emission of 155 R. This should however be confirmed by theoretical studies and/or laboratory measurements.

Because of the many unknown parameters of the Barth mechanism, a good fit of the green-line intensity is easily achieved, but it cannot validate the process (in contrast to the Earth's case, we do not have an altitude profile of the emission for Venus, but an integrated intensity of the green line). However, this mechanism cannot explain the variations of the green-line emission. To explain the variability of the infrared O_2 emission, Crisp et al. (1996) proposed several thermospheric effects, such as gravity waves, or O transport from the dayside to the nightside. If confirmed, such assumptions may overcome the intrinsic difficulties of the Barth mechanism, to account for the emission variability. Significant uncertainties, however, remain about the excitation state of the precursor in the Venusian mesosphere, and of the value of the quenching rate constant for CO_2.

A.2. The Slanger process

For both atmospheric and energetic reasons, Slanger et al. (2006b) proposed an alternative mechanism at low altitude:

$$O_2(c^1\Sigma_u^-, v = 0) + CO \rightarrow CO_2 + O(^1D,^1 S). \tag{A.11}$$

This reaction accounts for the fact that the $O_2(c^1\Sigma_u^-, v = 0)$ emission was observed in the atmosphere of Venus, but not the $O_2(c^1\Sigma_u^-, v \geq 2)$ emissions. This process takes place at altitudes where the Barth mechanism is efficient, i.e. close to 105 km, because the $O_2(c)$ state is derived indirectly from the Barth process, as described in Parisot (1986). This reaction cannot again explain the intensity variability. Moreover, it has never been observed nor suggested in other studies. Although it cannot be ruled out, dedicated experiments must be carried out to validate this reaction.

A.3. The O_{2^+} + N process

In Langford et al. (1986), experimental results shows that the $N^+ + O_2 \rightarrow NO^+ + O(^1S)$ or $O(^1D)$ reaction can take place. This (surprising) chemical reaction, given an excited state, is explained by the correlation diagram from Katsumata et al. (1982). The reaction giving $O(^1S)$ is less exoergic and does not exhibit a direct correlation, but is observed. This reactions were used to model the auroral emission, and it was found that the one giving $O(^1D)$ can explain ≈10% of the red line (Langford et al. 1985). We used these reactions to model the nightside red and green line of Venus, by using the N^+ densities measured by Pioneer Venus Orbiter. However, the N^+ density is so small that this reaction accounts for less than one percent of the emission.

Frederick et al. (1976); Kopp et al. (1977) propose a similar kind of reactions: $O_2^+ + N \rightarrow O(^1S) + NO^+$, to explain the Terrestrial green-line emission at high altitude. Although similar to the Langford reaction, the Frederick/Kopp reaction has several points that need to be studied:

- The first point is that $N(^4S) + O_2^+(X^2\Pi_g) \rightarrow NO^+(X^1\Sigma_g^+) + O(^1S)$ is spin-forbidden. However many cases of spin-forbidden reactions are known to occur with good efficiency because of strong spin-orbit couplings (Scott et al. 1998).
- The second point is that this reaction has several more exoergic channels, in particular the spin-allowed $NO^+(X^1\Sigma_g^+) + O(^3P)$ channel. Those exoergic channels are expected to be statistically strongly favoured compared to the less exoergic $NO^+ + O(^1S)$ channel (0.1 eV). However Smith et al. (1983) states that "the propensity to deliver a substantial fraction of the reaction exothermicity into electronic excitation of the atomic product appears to be a somewhat general phenomenon". The relative importance of these channels has then to be thoroughly investigated.
- The third point is that the qualitative correlation diagram published by Langford et al. (1986) based on NO_2^+ energies from Katsumata et al. (1982) shows no direct correlation between the $O_2^+ + N$ and $O(^1S) + NO^+$ channel. This seems to imply the existence of an energetic barrier entrance channel of this reaction. However if such a barrier exists, the reaction can become important if one of the reactant has kinetic energy. Indeed, many experiments show that the reaction rates are drastically modified when the reactants have even a very low kinetic energy (Alcaraz et al. 2004). As N comes from the dissociation of N_2 it could easily have kinetic energy, and several processes contribute to transfer kinetic energy to the ions in the planetary ionospheres.

It is clear that the $O_2^+ + N \rightarrow O(^1S) + NO^+$ reaction proposed in Frederick et al. (1976) needs further investigation, and especially laboratory measurements. If this reaction turns out to be impossible, it will be necessary to seek an alternative interpretation of the Earth's thermospheric observations (well above the Barth's mechanism efficiency layer), and to explain the variability of the green-line emission, both at Earth and Venus. $N^+ + O_2$ is a candidate that has already been observed (Langford et al. 1985). However, this reaction may hardly account for the observations because of the low density of N^+. The reaction $N(^3P) + O_2$ cannot explain the green line because the amount of $N(^3P)$ is too low. There may exist another set of reactions that create $O(^1S)$. The importance of these reactions will depend on the densities of the reactants in their specific excited state. Finally these reactions may also be specific to the chemistry of the planet considered.